

## Origin of the Improved Performance of High-Deposition-Rate Microcrystalline Silicon Solar Cells by High-Pressure Glow Discharge

Takuya MATSUI\*, Michio KONDO and Akihisa MATSUDA

National Institute of Advanced Industrial Science and Technology (AIST), 1-1-1 Umezono, Tsukuba, Ibaraki 305-8568, Japan.

(Received June 2, 2003; accepted for publication June 6, 2003)

We have demonstrated that a high-pressure process in  $\text{SiH}_4\text{-H}_2$  glow discharge provides highly efficient ( $\sim 8\%$ ) microcrystalline silicon ( $\mu\text{-Si:H}$ )  $p\text{-}i\text{-}n$  solar cells at  $i$  layer deposition rates of 2-3nm/s. In such a high-deposition-rate regime, we observed a remarkable improvement in visible-infrared responses upon increasing deposition pressure (up to 7-8 Torr), yielding high short circuit current. Transmission electron microscopy and secondary ion mass spectroscopy studies reveal that the high-pressure process provides denser grain columns coalesced with [110]-oriented crystallites, whereas samples prepared at lower pressure comprise many grain boundaries due to disordered grain growth, which induces atmospheric impurity diffusion in large concentrations. Reduction in post-oxidation associated with the denser microstructure of high-pressure-grown  $\mu\text{-Si:H}$  is responsible for the excellent charge collection behavior  $p\text{-}i\text{-}n$  structures. [DOI: 10.1143/JJAP.42.L901]

KEYWORDS: microcrystalline silicon, PECVD, high-rate deposition, solar cell microstructure, post-oxidation

Hydrogenated microcrystalline silicon ( $\mu\text{-Si:H}$ ) films for photovoltaic application are of considerable current interest because of their wide-range spectral sensitivities and excellent stabilities against light exposure. In the last decade, remarkable progress in solar cell efficiency has been achieved employing low-temperature ( $\sim 200^\circ\text{C}$ ) deposition techniques such as plasma-enhanced chemical vapor deposition (PECVD)<sup>1-5</sup> and hot-wire chemical vapor deposition.<sup>6</sup> Since  $\mu\text{-Si:H}$  is an indirect band gap material, solar cell requires a relatively thick absorber layer (at least  $2\mu\text{m}$  with light trapping) to gain sufficient low-energy-photon absorption. However, high-efficiency ( $>8\%$ )  $\mu\text{-Si:H}$  solar cells reported so far can only be achieved at limited deposition rates typically as low as 0.5nm/s. Consequently, a high-rate deposition technique for the  $\mu\text{-Si:H}$  solar cell is essential in view of future industrial mass production.

In the PECVD process using a  $\text{SiH}_4\text{-H}_2$  gas mixture, high-rate  $\mu\text{-Si:H}$  deposition requires a high flux of precursor radicals (such as  $\text{SiH}_3$ ) and a sufficient flux of atomic H per monolayer deposition,<sup>7</sup> which are realized in a high-discharge-power regime. Under conventional low pressure conditions ( $\sim 1\text{Torr}$ ), however, increasing discharge power deteriorates both film crystallinity<sup>8</sup> and solar cell performance.<sup>9</sup> This adverse effect has been attributed to the high-energy bombarding of ionic species due to enhanced electron temperature.<sup>7,8</sup> Recently, we have developed a novel PECVD technique under high gaseous pressures for reducing electron

temperature in a high rate  $\mu\text{-Si:H}$  deposition process.<sup>8</sup> The emphasis of this technique is placed on employing the  $\text{SiH}_4$  depletion regime where  $\text{SiH}_4$  molecules are efficiently decomposed and hence the H annihilation reaction,  $\text{SiH}_4 + \text{H} \rightarrow \text{SiH}_3 + \text{H}_2$ , is suppressed. Combining with the state-of-the-art very high frequency (VHF) discharge technology,<sup>10</sup> which enables faster growth of  $\mu\text{-Si:H}$  than conventional 13.56MHz rf-discharge, more than 5nm/s  $\mu\text{-Si:H}$  deposition has been reported.<sup>8</sup>

In spite of the achievement of high-rate  $\mu\text{-Si:H}$  deposition, only few studies have been made to identify its applicability to solar cell fabrication.<sup>4,11</sup> Furthermore, a detailed investigation on the material properties and device performance of high-deposition-rate  $\mu\text{-Si:H}$  has been lacking. In this letter, we demonstrate  $\sim 8\%$  efficient  $\mu\text{-Si:H}$   $p\text{-}i\text{-}n$  solar cells prepared at deposition rates of 2-3nm/s using high-pressure glow discharge. We further investigate the microstructure and impurity contamination level of  $\mu\text{-Si:H}$  films prepared at different deposition pressures. As a result, we found a strong connection between these material properties and solar cell performance.

The solar cells employed in this study consist of glass/ZnO (textured)/ $p\text{-}i\text{-}n$ /ZnO/Ag multilayers with an active area of  $0.25\text{cm}^2$ . All  $\mu\text{-Si:H}$   $p$ -( $\sim 25\text{nm}$ ),  $i$ -( $2.2\text{-}2.4\mu\text{m}$ ), and  $n$ -( $30\text{nm}$ ) layers were subsequently deposited by capacitively coupled 70-100MHz PECVD in an ultrahigh vacuum (UHV) multichamber system at a background pressure of less than  $3 \times 10^{-10}\text{Torr}$  and a reactor buildup rate of as low as  $1.2 \times 10^{-8}$

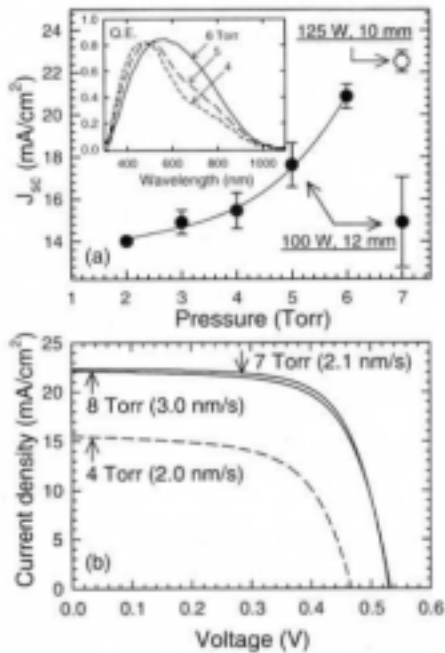


Fig. 1. (a): Short circuit current density  $J_{sc}$  of  $\mu\text{-Si:H}$  solar cells as a function of  $i$  layer deposition pressure for two different sets of discharge powers  $P_{rf}$  and anode-cathode spacings  $d$  (closed:  $P_{rf} = 100\text{ W}$ ,  $d = 12\text{ mm}$ ; open:  $P_{rf} = 125\text{ W}$ ,  $d = 10\text{ mm}$ ). The inset shows pressure dependence of quantum efficiency spectra of  $\mu\text{-Si:H}$  solar cells. (b):  $J$ - $V$  characteristics of  $\mu\text{-Si:H}$  solar cells prepared at different deposition pressures (solid lines: 7 and 8 Torr, dashed line: 4 Torr).

Torr  $\cdot$  //s. The  $\mu\text{-Si:H}$   $i$  layers were deposited at 160 using a  $\text{SiH}_4\text{-H}_2$  gas mixture at a constant  $\text{SiH}_4/\text{H}_2$  flow rate ratio of 9/510. The deposition pressure was varied in the range of 2-7Torr, while the discharge power and anode-cathode spacing were simultaneously adjusted to maintain the deposition rate at  $\sim 2\text{ nm/s}$ . The solar cells were characterized by current-voltage ( $J$ - $V$ ) and spectral response measurements under standard air mass 1.5 ( $100\text{ mW/cm}^2$ ) and white-biased monochromatic light illuminations, respectively.

The microstructure of  $\mu\text{-Si:H}$   $i$  layers was investigated by cross-sectional transmission electron microscopy (TEM) in a JEOL JEM-2000EX operated at an acceleration voltage of 200kV. The (220) Bragg electron diffraction beams were used for the dark-field images. X-ray diffractometry (XRD) in a  $\theta$ - $2\theta$  geometry was carried out to confirm the crystallographic orientation of the films. The film crystallinity of  $\mu\text{-Si:H}$   $i$  layers was also evaluated by Raman scattering spectroscopy using a He-Ne 633nm excitation source.

Figure 1(a) shows the short circuit current density  $J_{sc}$  of  $\mu\text{-Si:H}$  solar cells a function of  $i$  layer deposition pressure in the range of 2-7Torr. At a constant discharge power  $P_{rf} = 100\text{ W}$  and an anode-cathode spacing  $d = 12\text{ mm}$ , deposition rate of  $i$  layer takes a maximum at 4Torr and it varies within 1.1-2.0nm/s in the investigated pressure range. In Fig. 1(a),  $J_{sc}$  shows a monotonic increase with an increase in deposition

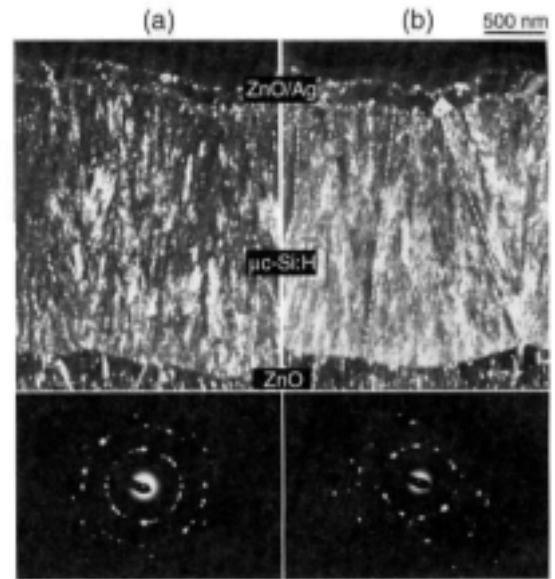


Fig. 2. Dark-field cross-sectional TEM images and corresponding SAD patterns of  $\mu\text{-Si:H}$  solar cells prepared at  $i$  layer deposition pressures of (a) 4 Torr ( $P_{rf} = 100\text{ W}$ ,  $d = 12\text{ mm}$ ) and (b) 7 Torr ( $P_{rf} = 125\text{ W}$ ,  $d = 10\text{ mm}$ ). Bright regions correspond to (220) Si crystallites oriented normal to the substrate. In (b), dashed lines indicate grain boundaries that separate large grain columns.

pressure up to 6Torr. This arises from the remarkable improvement in the quantum efficiencies at longer wavelengths ( $>600\text{ nm}$ ) as shown in the inset. With further increasing pressure up to 7Torr,  $J_{sc}$  rapidly drops down to a significantly lower value, which can be attributed to the phase transition from microcrystalline to amorphous growth as determined from Raman and XRD measurements. Nevertheless,  $J_{sc}$  markedly increases when using higher  $P_{rf} = 125\text{ W}$  and narrower  $d = 10\text{ mm}$ . As a result, the highest conversion efficiency  $\eta = 8.2\%$  ( $J_{sc} = 22.3\text{ mA/cm}^2$ , open circuit voltage  $V_{oc} = 0.53\text{ V}$ , and fill factor  $FF = 0.69$ ) has been obtained at 7Torr deposition at a deposition rate of 2.1nm/s. After the strict optimization of electrode spacing ( $d = 8\text{ mm}$ ) and  $\text{SiH}_4$  flow rate ( $\text{SiH}_4 = 12/680$ ), we have achieved  $\eta = 7.9\%$  ( $J_{sc} = 22.1\text{ mA/cm}^2$ ,  $V_{oc} = 0.53\text{ V}$ , and  $FF = 0.67$ ) at 8Torr deposition at a higher deposition rate of 3nm/s. The  $J$ - $V$  characteristics of these two solar cells are shown in Fig. 1(b), together with that obtained at 4Torr deposition for comparison. The results clearly demonstrate that the high-pressure  $\mu\text{-Si:H}$  deposition is quite effective in obtaining high performance solar cells at high deposition rates.

TEM studies reveal an appreciable difference in microstructure between  $\mu\text{-Si:H}$  films deposited at low and high pressures. Figure 2 shows the dark-field cross-sectional TEM images and selected area (focused on the film-substrate interface of 100nm diameter) diffraction (SAD) patterns of two  $\mu\text{-Si:H}$  samples chosen from the pressure series shown in Fig. 1: (a) 4Torr ( $P_{rf} = 100\text{ W}$  and  $d = 12\text{ mm}$ ) and (b) 7Torr ( $P_{rf} = 125\text{ W}$  and  $d$

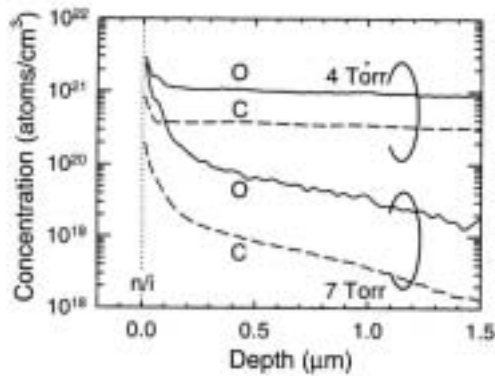


Fig. 3. Oxygen (solid) and carbon (dashed) SIMS depth profiles of  $\mu\text{c-Si:H}$  solar cells prepared at different  $i$  layer deposition pressures. SIMS points near the film-substrate ( $p/i$ ) interface are not shown due to a strong oxygen signal from a roughly-textured ZnO-coated substrate.

=10mm). For both dark-field TEM micrographs, bright regions correspond to (220) crystalline grains oriented normal to the substrate. As shown in Fig. 2(a), the  $\mu\text{c-Si:H}$  film prepared at low pressure is composed of fiber like crystalline grains with lateral sizes of 50-80nm. In addition, each grain is found to grow disconnectedly and the maximum grain length is determined to be  $\sim 500\text{nm}$ , which is much shorter than the film thickness. In the corresponding SAD pattern, superposition of several diffraction spots is observed along the inner three Debye-Scherrer rings corresponding to Si (111), (220) and (311) reflections, indicative of disordered distribution of crystallographic orientation. In contrast, as shown in Fig. 2(b), the  $\mu\text{c-Si:H}$  film prepared at high pressure shows a denser grain arrangement coalesced with oriented crystallites that extend over the entire film thickness. Such crystalline growth appears to form wide grain columns approximately  $1\ \mu\text{m}$  in lateral size separated by some prominent grain boundaries (indicated by dashed lines). The formation of these grain boundaries originates from the grain collision induced by the surface texture of the ZnO substrate.<sup>4)</sup> The characteristic spotty SAD pattern arranged by coherently scattering domains provides further evidence of large grains with preferential orientation.

Above TEM observations are consistent with our XRD results that a structural change occurs from random to (220) preferential orientation as the deposition pressure increases. On the other hand, we observed no significant difference in both crystalline ( $520\text{cm}^{-1}$ ) and amorphous ( $480\text{cm}^{-1}$ ) peaks in the Raman spectra between two samples investigated in TEM. In addition, electron spin resonance study reveals low dangling-bond densities of less than  $9 \times 10^{15}\text{cm}^{-3}$ , independent of deposition pressure. Accordingly, these material properties suggest that solar cell performance is predominantly

determined by the crystallographic microstructure including preferential orientation rather than by the crystalline volume fraction or defect density in the film. A similar microstructural dependence of solar cell performance has been reported for low-deposition-rate ( $<0.4\text{nm/s}$ ) samples, in which (220) preferential orientation is proposed to provide high-efficiency solar cells.<sup>12)</sup> It has been pointed out that the [110]-oriented silicon contains [110]-tilt boundaries which are electrically inactive and therefore beneficial for solar cells.<sup>13)</sup> However, the role of the microstructure played in  $\mu\text{c-Si:H}$  solar cell performance has not been fully addressed.

We find a correlation between the microstructure and atmospheric impurity diffusion behavior in  $\mu\text{c-Si:H}$  films. Figure 3 shows the secondary ion mass spectroscopy (SIMS) profiles of oxygen and carbon measured on two distinct  $\mu\text{c-Si:H}$  solar cells identical to those investigated in TEM. Note that these SIMS measurements were performed about two months after cell fabrication and characterization. As is evident from Fig.3, oxygen and carbon impurities in  $\mu\text{c-Si:H}$  prepared at high pressure show a gradual decrease in the film, whereas those in  $\mu\text{c-Si:H}$  prepared at low pressure extend throughout the entire film thickness in larger concentrations. At the film-substrate interface region, the impurity level differs by two orders of magnitude. Since the UHV deposition system was employed in this study, we can exclude the possibility that such anomalous impurity incorporation occurs during the film growth. Thus, the SIMS results suggest that atmospheric impurities diffuse from the top surface after air exposure. We attribute the enhanced impurity diffusion found for low-pressure-grown  $\mu\text{c-Si:H}$  to the increased grain boundaries as suggested by TEM shown Fig.2 (a).

Oxygen in  $\mu\text{c-Si:H}$  film is widely known to create shallow donor states at grain boundaries in higher efficiencies compared to amorphous silicon based semiconductors.<sup>13,14)</sup> This undesirable effect makes undoped  $\mu\text{c-Si:H}$  films to exhibit strong  $n$ -type character. Torres *et al.* reported that the spectral response of the  $\mu\text{c-Si:H}$  solar cells with an intentionally contaminated  $i$  layer (oxygen:  $2.2 \times 10^{20}\text{atoms/cm}^3$ ) shows a significant absence of IR response,<sup>14)</sup> in agreement with that of our low-pressure-grown  $\mu\text{c-Si:H}$  solar cells shown in the inset of Fig. 1 (a). Those characteristic quantum efficiency spectra, i.e., high blue response and low IR response, imply that the built-in field localizes at the  $p/i$  interface due to  $n$ -type character of  $i$  layer.<sup>5)</sup> Furthermore, we observed an irreversible cell degradation behavior for low-pressure-grown  $\mu\text{c-Si:H}$ . Measuring two months after deposition,  $J_{\text{sc}}$  was found to decrease by approximately 50% compared to the initial values and the quantum efficiency spectra showed almost no IR response. In contrast, high-pressure-grown samples did not

show any degradation. These results suggest that oxygen diffusion and post-oxidation are most responsible for the reduction in  $J_{sc}$  for randomly oriented  $\mu\text{-Si:H}$  solar cells prepared at low deposition pressures.

In conclusion, we have shown that deposition pressure plays a dominant role in determining  $J_{sc}$  of  $\mu\text{-Si:H}$  solar cells fabricated using a high-deposition-rate PECVD process. High-pressure deposition at more than 7Torr is found to be advantageous in obtaining high  $J_{sc}$ . As a result,  $\eta = 8.2\%$  and  $7.9\%$  are achieved at deposition rates of 2.1 and 3.0nm/s, respectively. We proposed that reduction in post-oxidation associated with the denser microstructure of high-pressure-grown  $\mu\text{-Si:H}$  is responsible for the excellent charge collection behavior in  $p\text{-i-n}$  solar cell structures.

The authors acknowledge research support from the New Energy and Industrial Technology Development Organization (NEDO), Japan.

- 1) J. Meier, s Dubail, R. Flükiger, H. Keoover and A. Shah: Appl. Phys. Lett. **65** (1994) 860.
- 2) K. Yamamoto: IEEE Treans. Electron Devices **46** (1999) 2041.
- 3) K. Saito, M. Sano, A. Sasaki, R. Hayashi and L. Ogawa: *Tech. Dig. 20th Int. PVSEC, jeju, Korea (Kyung Hee Information printing, Seoul 2001) p. 429.*
- 4) Y. Nasuno, M. Kondo and A. Matsuda: Jpn. J. Appl. Phys. **41** (2002) 5912.
- 5) T. Matsui, R. Muhida, T. Kawamura, T. Toyama, H. Okamoto, T. Yamazaki, S. Honda, H. Takakuda and Y. Hamakawa: Appl. Phys. Lett. **81** (2002)4751.
- 6) S. Klein, F. Finger, R. Carius, B. Rech, L. Houben, M. Luysberg and M. Stutzmann: Mater. Res. Soc. Symp. Proc. **715** (2002) A26.2.
- 7) A. Matsuda: J. Non-Cryst. Solids **59/60** (1983) 767.
- 8) M. Kondo, M. Fukawa, L. Guo and A. Matsuda: J. Non-Cryst. Solids **266-269** (2002) 84.
- 9) O. Vetterl, F. Finger, R. Carius, P. Hapke, L. Houben, O. Kluth, A. Lambertz, A. Muck, B. Rech and H. Wagner: Sol. Energy Mater. & Sol. Cells **62** (2000) 97.
- 10) F. Finger, U. Kroll, V. Viret, A. Shah, W. Beyer, X.-M. Tang, J. Weber, A. Howling and Ch. Hollenstein: J. Appl. Phys. **71** (1992) 5665.
- 11) T. Roschek, T. Repmann, J. Müller, B. Rech and H. Wagner: J. Vac. Sci. & Technol. A **20** (2002) 492.
- 12) T. Matsui, M. Tsukiji, H. Saika, T. Toyama and H. Okamoto: Jpn. J. Appl. Phys. **41** (2002) 20.
- 13) J. H. Werner, R. Dassow, T. J. Köhler and R. B. Bergmann: Thin Solid Films **383** (2001) 95.  
P. Torres, J. Meier, R. Flückiger, U. Kroll, J. A. Anna Selvan, H. Keppner, A. Shah, S. D. Littlewood, I. E. Kelly and P. Giannelis: Appl. Phys. Lett. **69** (1996) 1373.